Çukurova Üniversitesi Mühendislik Fakültesi Dergisi, 37(3), ss. 813-826, Eylül 2022
Cukurova University Journal of the Faculty of Engineering, 37(3), pp. 813-826, September 2022

Investigation of the Effect of Side Devices and Crosswind Flow on Aerodynamic Drag of a Ground Vehicle

Ahmet ŞUMNU[*1] **ORCID** *0000-0002-5580-5266*

[1]*İskenderun Technical University, Faculty of Aeronautics and Astronautics Engineering, Department of Aerospace Engineering, İskenderun*

Geliş tarihi: 11.05.2022 Kabul tarihi: 23.09.2022

Atıf şekli/ How to cite: ŞUMNU, A., (2022). Investigation of the Effect of Side Devices and Crosswind Flow on Aerodynamic Drag of a Ground Vehicle. Çukurova Üniversitesi, Mühendislik Fakültesi Dergisi, 37(3), 813-826.

Abstract

In the present study, effect of side devices and crosswind flow are investigated to observe aerodynamic drag coefficient for a simplified ground vehicle (Ahmed body) since it directly effects fuel consumption. When the literature was examined, the studies that were investigated effect of slant angle, velocity and geometric modifications were presented. However, there are few studies that proposed both side device effect and crosswind flow for ground vehicles at different yaw angles. The CFD (Computational Fluid Dynamic) solution is performed both model with side devices and crosswind flow condition. The crosswind flow condition has been analyzed at different yaw angles (β=5°, 10°, 20°, and 30°) to observe how to affected drag coefficient. Pressure contours have been presented for model with and without side devices and under the crosswind flow conditions at rear region of body since the most of the drag force occurs flow separation or adverse pressure gradient. The streamlines velocities have been presented at x-plane which is positioned side devices location under the crosswind flow conditions. In addition, vorticity magnitude has been given for both models with and without side devices at different yaw angle. In the results of study are observed that side devices adversely effects aerodynamic performance since flow separation occurs on the side of body and it causes to increase pressure drag. The pressure drop is also observed at rear region of model due to crosswind flow condition. This causes the increase of drag forces.

Keywords: Ahmed body, CFD, Flow separation, Yaw angle, Drag coefficient

Bir Kara Aracının Aerodinamik Sürüklenmesi Üzerine Yan Cihazların ve Yan Rüzgâr Akışının Etkisinin İncelenmesi

Öz

Bu çalışmada, yakıt tüketimini doğrudan etkilediği için basitleştirilmiş bir kara aracının (Ahmed gövdesi) aerodinamik sürükleme katsayısını gözlemlemek için yan cihazların ve yan rüzgâr akışının etkisi araştırılmıştır. Literatür incelendiğinde eğik açı, hız ve geometrik modifikasyonların etkisini araştıran çalışmalar sunulmuştur. Ancak, kara araçları için farklı sapma açılarında hem yan cihaz etkisini hem de yan rüzgâr akışını öneren az sayıda çalışma bulunmaktadır. Bu nedenle, HAD (Hesaplamalı Akışkanlar Dinamiği) çözümü hem yan cihazlara sahip modelde hem de yan rüzgâr akış koşulunda

[*]Corresponding Author (Sorumlu Yazar): Ahmet ŞUMNU, *ahmet.sumnu@iste.edu.tr*

gerçekleştirilmiştir. Yan rüzgâr akış durumu, sürükleme katsayısının nasıl etkilendiğini gözlemlemek için farklı sapma açılarında (β=5°, 10°, 20° ve 30°) analiz edilmiştir. Sürükleme kuvvetinin büyük bir kısmı akış ayrılması veya ters basınç gradyanından dolayı meydana geldiğinden, yan cihazlara sahip olan ve olmayan modeller için ve yan rüzgâr akış koşulları altında gövdenin arka bölgesindeki basınç konturları sunulmuştur. Yan rüzgâr akış koşulları altında, yan cihazların konumlandığı x-düzleminde akım çizgilerinin hızları sunulmuştur. Ek olarak, girdap büyüklüğü, farklı sapma açılarında yan cihazları olan ve olmayan her iki model için de verilmiştir. Çalışma sonuçlarında, akış ayrılması meydana geldiği ve basınç direncinin artmasına neden olduğu için yan cihazların aerodinamik performansı olumsuz etkilediği gözlemlenmiştir. Yan rüzgâr akış durumu nedeniyle modelin arka bölgesinde de basınç düşüşü gözlemlenmiştir. Bu, sürükleme kuvvetlerinin artmasına neden olmaktadır.

Anahtar Kelimeler: Ahmed gövdesi, HAD, Akış ayrılması, Sapma açısı, Sürükleme katsayısı

1. INTRODUCTION

The investigation of aerodynamic forces is crucial issue for a ground vehicle since the fuel consumption stems from friction and drag force acting on body. Ground vehicles are used in under different conditions such as velocity and direction of air, rainy weather condition, pressure. Therefore, when the aerodynamic analysis is performed, all conditions are taken into account to find realistic and accurate results for experimental or analytic solutions. The previous studies are mentioned related with ground vehicles in the following paragraph.

Ahmed et al. [1] performed an experimental study for ground vehicle that is known Ahmed body, to analyze the wake structure at different slant angle. The results of this study showed that the flow separation and wake flow cause increase in dag force. The investigation of different shape of rear region of vehicle was performed in terms of aerodynamic performance in a wind tunnel [2]. Lienhart and Becker [3] also investigated contribution of wake generation on aerodynamic drag at behind of the simplified car model. Watkins and Vino [4] performed the study on Ahmed body aerodynamics by positioning the two co-linear bodies. It was deduced that the effect of space of two bodies significantly increase drag coefficients and strong vortex formation that cause the change of drag and lift force at rear region of body was observed. Another study was performed to investigate aerodynamic of Ahmed body using experimental and numerical method by Meile et al. [5]. Large Eddy Simulation (LES) method was used to perform numerical simulation of Ahmed body at high Reynolds-number by Östh et al. [6]. In order to observe unsteady wake occurring on Ahmed model, experimental study was performed by Volpe et al. [7].

In real case, an automobile is generally exposed to crosswind. Therefore, crosswind conditions should be taken into account when aerodynamic analysis is performed. In the literature, there are few studies related with this issue. The crosswind sensitivity was investigated to decide how to effect the ground vehicle aerodynamics and driving performance by [8]. Ahmed body model was used to perform analysis at 0°-15° yaw angle and 25° and 35° slant angle. It was deduced that rate of turbulence and velocity fluctuations were significantly effect the shear layers so, rear vertical and slanted surface were important in terms of flow dynamics. Heavy ground vehicles was presented to investigate crosswind effect because they have high lateral surface area and center of gravity of heavy vehicles are higher above ground than an automobile [9]. Crosswind effect was investigated to observe aerodynamic characteristic at different yaw angles for long vehicles and heavy vehicles by [10]. The study applied crosswind over Ahmed body was implemented using rear cavities at base body [11]. The crosswind effect was also investigated to evaluate aerodynamic performance using different shape body and wind tunnel test [12]. Both experimental and numerical studies were performed for observation of crosswind conditions on bluff bodies at 0° to 30° yaw angles [13]. In addition, the similar analysis was carried out using DES (Detached-Eddy Simulation) at 0°

to 30° yaw angles and it was concluded that the results were good agreement with experimental results [14]. Altınışık and Umur [15] focused on crosswind analysis for a special car. They performed wind tunnel test and numerical analysis to observe how to effect crosswind flow for selected car model. It was deduced that drag coefficient increased up to 35° yaw angle and after that point, drag coefficient become to reduce. Crosswind and headwind flow that is incompressible and unsteady was also analyzed for the Ahmed body [16]. Another study that was investigated yaw angle effects on aerodynamic performance was performed experimental study for Ahmed body [17]. It was deduced that drag coefficient was increase at yaw angle 0°- 60°. However, it remains constant between 60° and 75° and it then increase up to 90°.

The experimental study was implemented using particle image velocimetry (PIV) technique to investigate flow physics at different slant angle of Ahmed body [18]. The slant angle effect was observed for Ahmed body by means of numeric analysis and the results were compared experimental study [19].

Some devices that mounted on automobiles side or upper regions should be taken into consideration since these devices affect the aerodynamics of automobile body. However, when previous studies are examined, there are limited studies that take into account side devices effect on aerodynamics. Murutila et al. [20] presented a study adding a device that is side view mirrors to investigate the effects on the aerodynamic drag coefficients. It was deduced that drag coefficient was increase about % 6 for Ahmed body with slant angle 25°. The effect of rear view side mirrors was investigated for a car [21]. Four different models were generated and numerically analyzed to observe side devices effect.

Some devices can be used to improve aerodynamic performance of automobiles. These may be passive and active devices that use to control over the body. In the literature, some studies have been presented. Ahmed and Murtaza [22] presented the review study related with car aerodynamics and investigated effect of passive flow devices. The research results were concluded that the passive devices should be applied commercial vehicles and the aerodynamic noise study should be performed to enhance the quality of comfort. An active flow control study was presented to improve aerodynamic efficiency using jet actuator for Ahmed body [23]. It was deduced that drag force was reduced for 25° slant angle while drag force was increase for 35° slant angle. Buscariolo et al. [24] presented study for Ahmed body using diffuser and observed flow field that occurs on the rear region. The diffuser analysis was performed by changing the angle that is between 0° and 50°. It was concluded that change of drag and lift coefficient was %13 and %1, respectively. A study was proposed by Yakkundi and Mantha [25] to observe CFD solution and experimental study to validate for generated image model car. Demircioglu [26] proposed aerodynamic analysis of F1 race automobile to observe velocity and pressure distribution occurring over car body at 130 km/h. The similar study was performed for electric vehicles. Both numerical and experimental studies were carried out and the results were compared [27].

The unsteady analysis is performed, if we want the realistic results. Therefore, the solution can be performed time depended. The some previous studies mentioned unsteady analyses are presented in the following. Han [28] proposed numerical study to predict flow around the Ahmed model-like body very well. The Averaged-Reynolds Navier-Stokes equations were solved numerically together with k-ε turbulence model. The reverse flow region and trailing vortices was predicted for three dimensional turbulent flow of the Ahmed vehicle. Krastev and Bella [29] investigated steady and unsteady flow over the Ahmed body using open source CFD toolbox OPENFOAM. Using URANS and steady-state RANS model the numerical simulations were implemented and compared with experimental results available in the literature. Hinterberger et al [30] performed a study to investigate Ahmed body model with slant angle 25° using LES (Large Eddy Simulation).

Another similar study that performed experimentally to visualize longitudinal vortices that occurs the side edges of the rear window at 25° slant angle of Ahmed body model was presented by Jermann et al. [31].

Optimization studies have presented to improve the shape of the body for reduction of drag force and increase the efficiency in point of fuel consumption. When examined the previous studies, a paper was presented by Dumas [32]. The hybrid optimization that was combined a Genetic Algorithm (GA) and a second-order Broyden-Fletcher-Goldfarb-Shanno (BFGS) method were applied to the 3D car model for drag minimization. Beigmoradi et al. [33] performed optimization study based on aerodynamic and acoustic objectives. In this study, realizable k-ε turbulent model and broad band noise model was used to perform simulation of model. Taguchi method was also used to reduce number of simulation. The optimum results were obtained using Genetic Algorithm and Artificial Neural Network optimization method. He et al. [34] presented CFD based optimization combining adjoint approach and gradient based method for computing derivatives to optimize the designs. In order to show their optimization framework, bluff body with ramp shape geometry was optimized and the drag level reduced about 9%. The optimization study related with rear end of Ahmed body was proposed by Han et al. [35]. Three dimensional Navier-Stokes analyses were performed for optimization. The three items that backlight angle, boat-tail angle and ramp angle were investigated to find optimum shape for reduction of drag coefficient. The results showed that drag reduction was achieved about 0.13. Wang et al. [36] focus on optimization of Ahmed body for non-smooth surface on the drag reduction. In this study flow field analysis was performed and compared with experimental date in the literature then optimization method that multi-island Genetic Algorithm was applied to increase the efficiency in point of aerodynamic. Qiao et al. [37] presented to flow control for bluff body using multi-frequency and optimization was also performed to reduce drag coefficient value at 10° yaw angle. It was concluded that drag reduction was achieved about %20 by applying genetic algorithm optimization. In order to reduce aerodynamic drag coefficient, geometric revision on the analyzed car was performed and the results were observed that drag force and pressure on the car body were reduced and performance was improved [38].

The result of examined literature related with automobile aerodynamics, there are few studies about side effects with crosswind analysis. In addition, yaw angles of crosswind were generally studied at low, medium and high angles that are between 5° and 30° in previous studies. Therefore, in this study, the analysis of side devices with crosswind have been performed up to 30° yaw angle. The solution results are presented for both models with and without side devices under the crosswind condition to show how to affect the aerodynamic performance of simplified ground vehicle. The following sections are given to explain generation of body and mesh structure and CFD solutions setup in ANSYS.

2. COMPUTATIONAL SETUP

2.1. Geometry of Ahmed Body

In this study, the Ahmed body has been studied in point of aerodynamic analysis to investigate the side device and crosswind effects. For this, geometry was firstly generated using Designmodeler in ANSYS and mesh generation has been then performed Mesh in ANSYS. The dimensions of body are shown in Figure 1 [1,30]. Figure 2 shows solid model of the Ahmed body and Figure 3 shows the model with side devices and its position and dimensions. These position and dimensions are determined by examining the previous studies [20, 21].

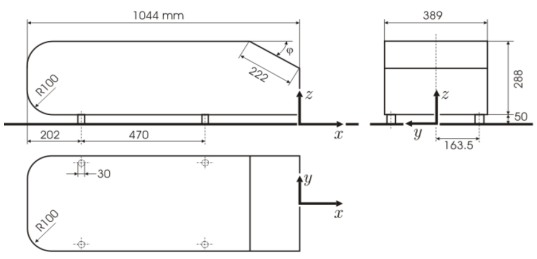

Figure 1. Dimensions of Ahmed body [1,30]

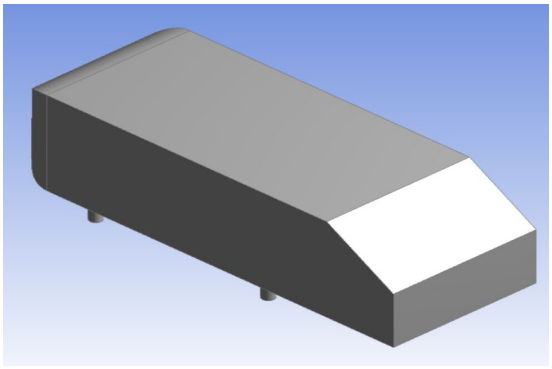

Figure 2. 3D view of Ahmed body

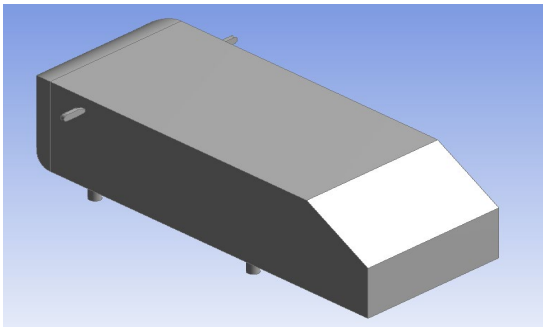

(a)

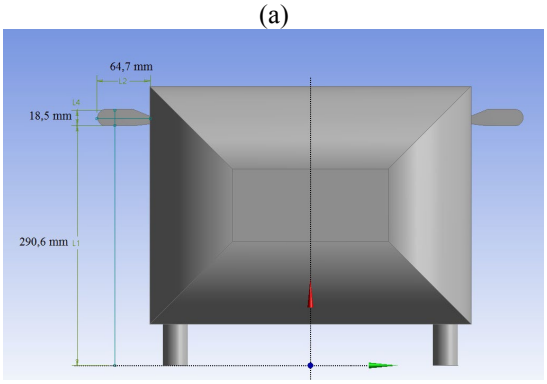

(b)

Figure 3. Ahmed body with side devices (a: Isometric view b: Front view with side device position and dimensions)

2.2 Mesh Generation

The mesh generation process is a crucial issue to obtain precision results. The number of mesh and generation method should be compatible to capture flow field around the body. Therefore, mesh generation is started from courser to finer mesh number and prismatic layer is formed around the model at different number of inflation layer for obtaining accurate results. Inflation control is important to capture the boundary layer since turbulent boundary layer is expected in the solution. The results are compared with experimental results for verification. Tetrahedral mesh has been then generated. Rectangular shape is generated around the body as computational fluid domain. Its length, height and wide of fluid domain are 12, 10 and 10 times of the body length, height and wide, respectively.

In this study, the mesh generation has been performed using Mesh ANSYS. Figure 4 and 5 show the mesh generation for body and computational domain, respectively. The other issue is mesh sensitivity analysis in order to find sufficient mesh number and correct result. Therefore, the CFD solution has been implemented starting from courser mesh numbers to finer mesh numbers. The mesh dependency analysis is given in Figure 6. The CFD solution has been performed from starting 100.000 mesh numbers to 6 Million mesh numbers. The results show that 4 Million mesh numbers has been enough to find accurate solutions.

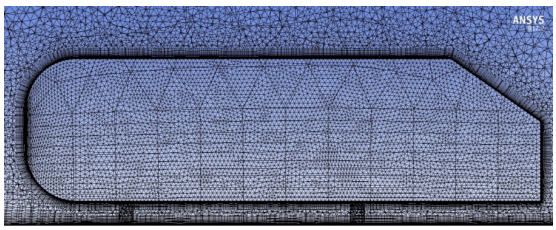

Figure 4. Mesh generation around the model

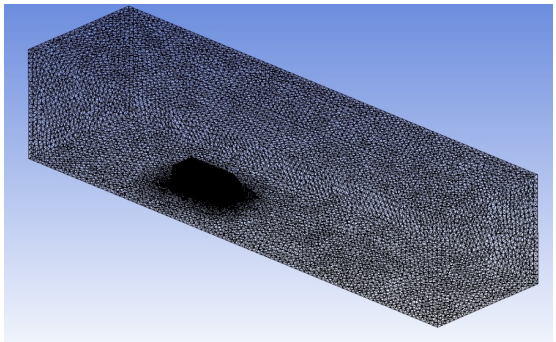

Figure 5. Mesh generation of computational fluid domain

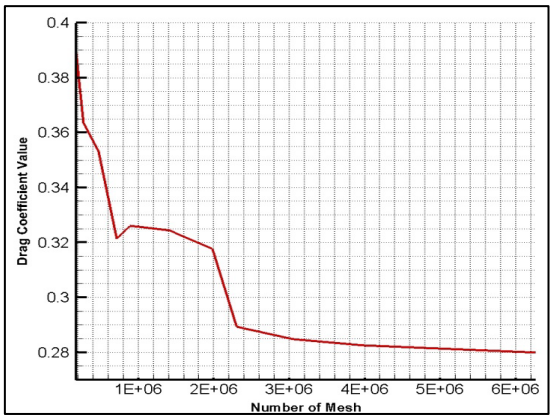

Figure.6. Mesh sensitivity analysis

2.3. Numeric Solution

The solution of the problem has been carried out using Fluent ANSYS that uses finite volume method. 3-Dimensional, steady, compressible solutions have been implemented. In order to describe the flow field, the Navier-Stokes equations that include the continuity and momentum equations are used.

The Navier-Stokes equation in x-direction can be written as (Equation 1)

$$\frac{\partial(\rho u)}{\partial t}+\nabla(\rho u V)=-\frac{\partial P}{\partial x}+\frac{\partial \tau_{xx}}{\partial x}+\frac{\partial \tau_{yx}}{\partial y}+\frac{\partial \tau_{zx}}{\partial z}+\rho fx \qquad (1)$$

In this study, RNG (Re-Normalisation Group) k-ε turbulence model was used since this turbulence model simulates accurately flow field for this specified conditions [39]. This model is renormalized the Navier-Stokes equations and take into account smaller motion effect. The RNG k-ε transport equation can be described as following (Equations 2 and 3).

$$\frac{\partial}{\partial t}(\rho k)+\frac{\partial}{\partial x_i}(\rho k u_i)=\frac{\partial}{\partial x_j}\left[\left(\mu+\frac{\mu_t}{\sigma_k}\right)\frac{\partial k}{\partial x_j}\right]+P_k-\rho\varepsilon \qquad (2)$$

$$\frac{\partial}{\partial t}(\rho\varepsilon)+\frac{\partial}{\partial x_i}(\rho\varepsilon u_i)=$$

$$\frac{\partial}{\partial x_i}\left[\left(\mu+\frac{\mu_t}{\sigma_\varepsilon}\right)\frac{\partial \varepsilon}{\partial x_i}\right]+C_{1\varepsilon}\frac{\varepsilon}{k}P_k+C_{2\varepsilon}^{*}\rho\frac{\varepsilon^2}{k} \qquad (3)$$

Where,

$$C_{2\varepsilon}^{*}=C_{2\varepsilon}+\frac{C_{\mu^3}\left(1-/_0\right)}{1+\beta^3}$$

$$\eta=Sk/$$

$$S=\left(2S_{ij}S_{ij}\right)^{1/2}$$

The setup of Fluent is defined as following. Ahmed body is described as wall type due to no-slip condition. During the solution, enclosure surfaces are defined as symmetry. Velocity-inlet is defined for inlet condition and pressure outlet is described for outlet plane. Solution method is selected as Roe-FDS flux type and flow is specified second order upwind. Solution is also implemented as density based and steady-state. Enhancement wall treatment is selected as the wall function for RNG k-ε turbulences model. Courant number is determined as 0.7. The dimensionless y^+ value is approximately "1" for capturing flowfield in boundary layer. However, some place on the body, it may be greater than 1. When the change of drag coefficient value is negligible small and the value of flow residuals reach to 10^{-5}, the solution run is finished. The CFD solutions are implemented at 40 m/s and different yaw angles (5°, 10°, 20°, 30°). Reynolds number that is based on model's length is $2.78x10^6$.

3. RESULTS AND DISCUSSION

In this study, crosswind and side device effects have been investigated for a simple ground vehicle. The analysis has been firstly performed without crosswind condition and side devices. When previous papers are examined, yaw angles of crosswind were generally studied at low, medium and high angles that are between 5° and 30°. Hence, solutions have been carried out by applying crosswind conditions at different yaw angles that is 5°, 10°, 20°, 30°. In addition, side

devices have been mounted on base model at position x= -0.8. All solutions have been carried out at 40 m/s velocity and 35° slant angle.

The pressure contours is presented at plane z=0 for rear region of body without side devices at yaw angle 0°, 5°, 10°, 20°, 30° in Figure 7. The range of pressure value is same for all figures since the comparison and observation can be made easily. When examined these figures and compared each other, it can be observed that pressure drop or adverse pressure gradient occur at rear region of body with increasing yaw angle of flow. In addition, it can be said that crosswind flow is especially affected at yaw angle 20° and 30° and pressure differences increase between front and rear region of model when compared with flow at 0° yaw angle. The flow separation can occur due to adverse pressure gradient formation and the flow cannot proceed over surface due to no-slip condition. This causes an increase in drag force for a ground vehicle. The pressure contours is presented at plane z=0 for rear region of body with side devices at yaw angle 0°, 5°, 10°, 20°, 30° in Figure 8. These figures are presented to observe the effect of side devices at rear region flow field by comparing with Figures 7. When the figures presented model with side devices can be observed that pressure drop at slant surface is more than model without side devices. In addition, it can be stated that side devices effect causes earlier flow separation due to adverse pressure gradient. Therefore, both crosswind and side device are adversely affect flow field at rear region and cause increase drag force.

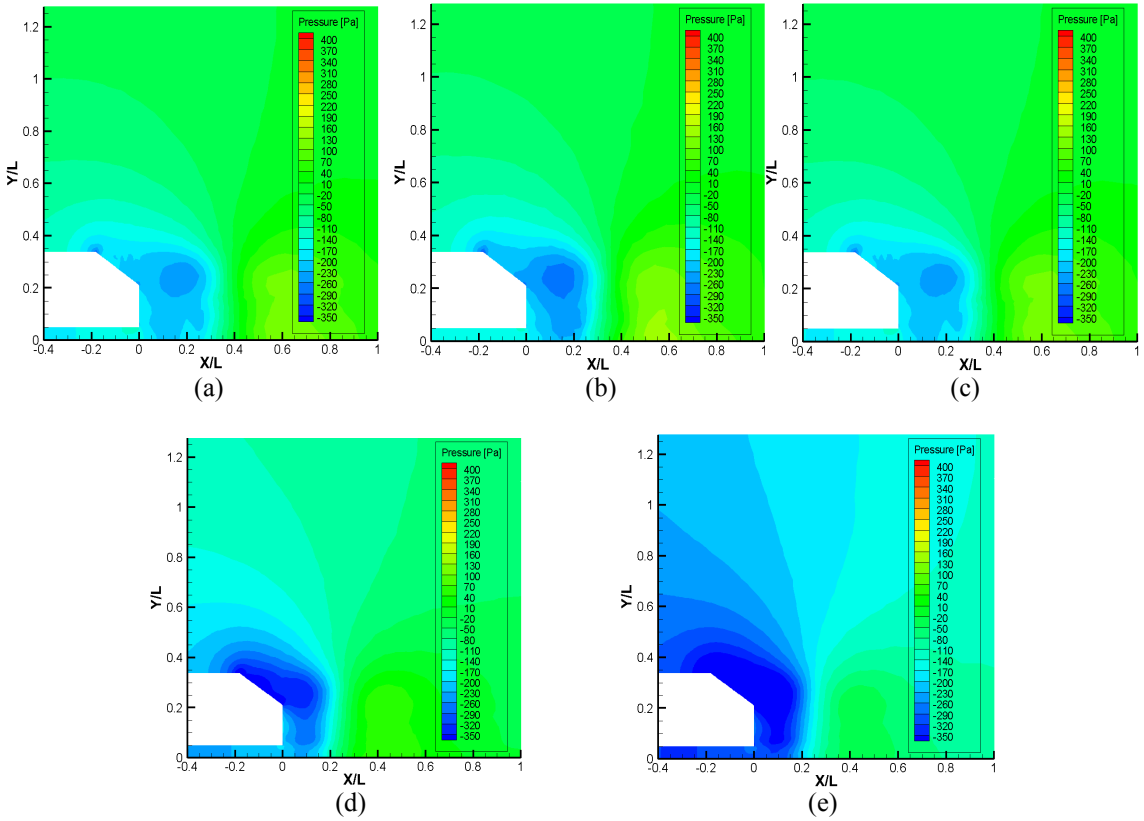

Figure 7. Pressure contours plane z=0 for rear region of body without side devices at 40 m/s and 35° Slant angle (a: yaw angle 0°, b: yaw angle 5°, c: yaw angle 10°, d: yaw angle 20°, e: yaw angle 30°)

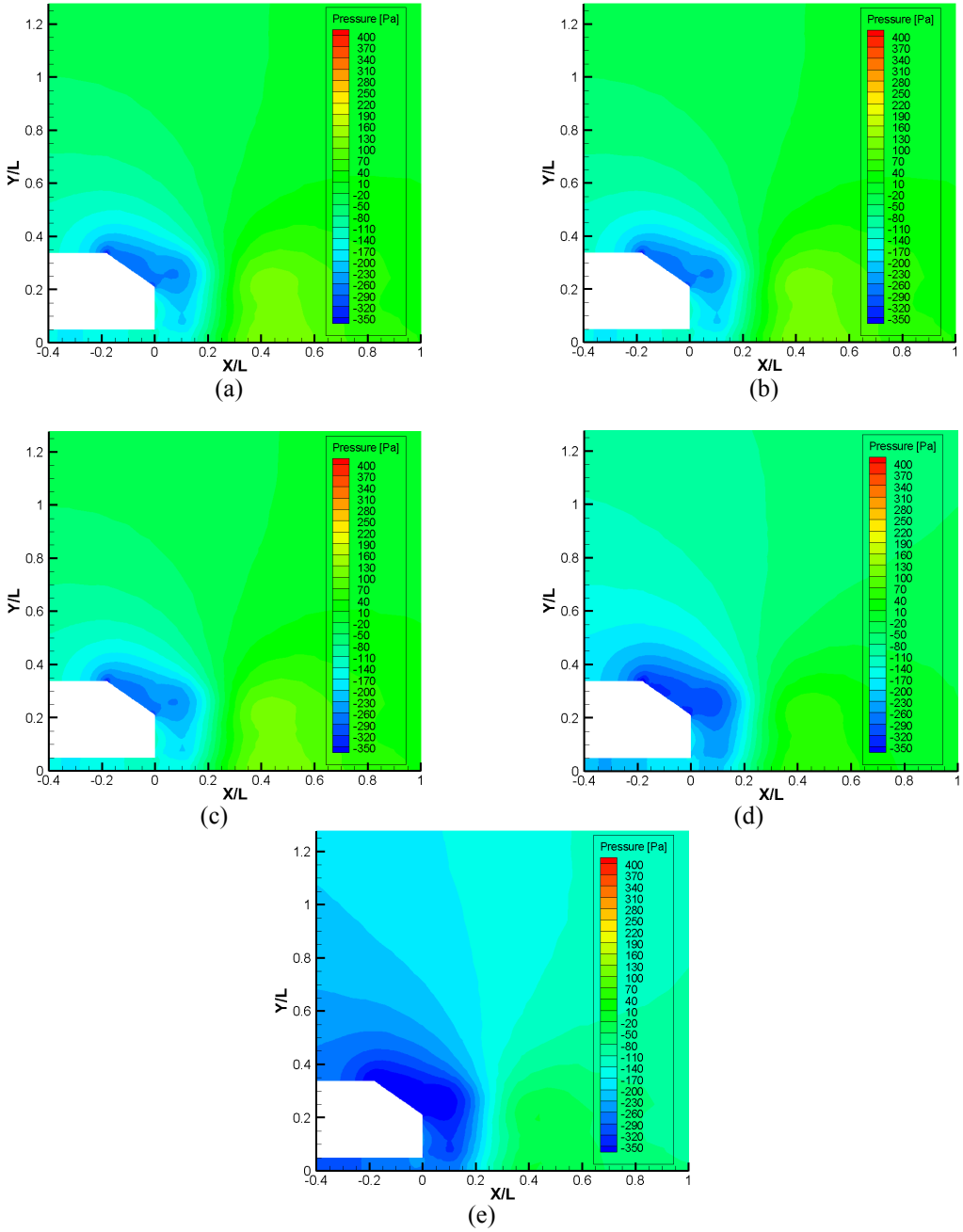

Figure 8. Pressure contours plane z=0 for rear region of body with side devices at 40 m/s and 35° Slant angle (a: yaw angle 0°, b: yaw angle 5°, c: yaw angle 10°, d: yaw angle 20°, e: yaw angle 30°)

The velocity streamlines are presented to show flow separation and vortices with and without side devices in Figure 9 and Figure 10, respectively. These streamlines are examined plane x=-0.8 which describes according to reference point that rear end of model. The vortex intensity and its

effected area increase with increasing yaw angle when examined the Figure 9. Moreover, flow separation and vortex generation can be observed over the top surface of model at yaw angles 10°, 20°, and 30° when compared with Figure 9(a) that represents flow without yaw angle. The Figure 10 represents the side devices position to show flow field. When examined these figures, side devices effect flow field as seen in Figures. However, it can be stated that the vortex area decrease when compared with solution results without side devices. Hence, it can be inferred that drag force does not significantly increase at mounted position of side devices but it may increase due to pressure drop behind side devices position as understood from figures.

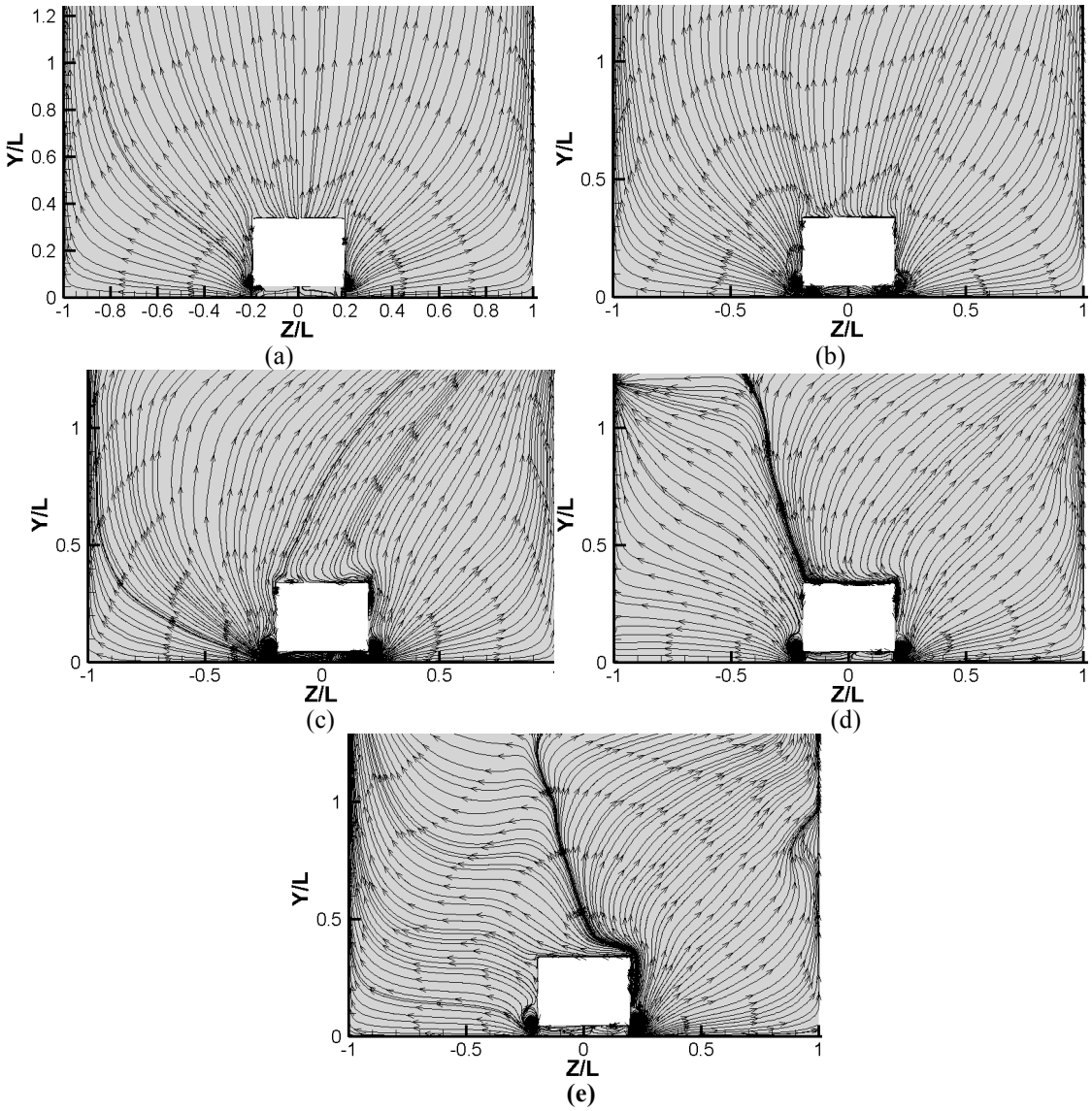

Figure 9. Streamlines velocity plane x=-0.8 for body without side devices at 40 m/s and 35° Slant angle (a: yaw angle 0°, b: yaw angle 5°, c: yaw angle 10°, d: yaw angle 20°, e: yaw angle 30°)

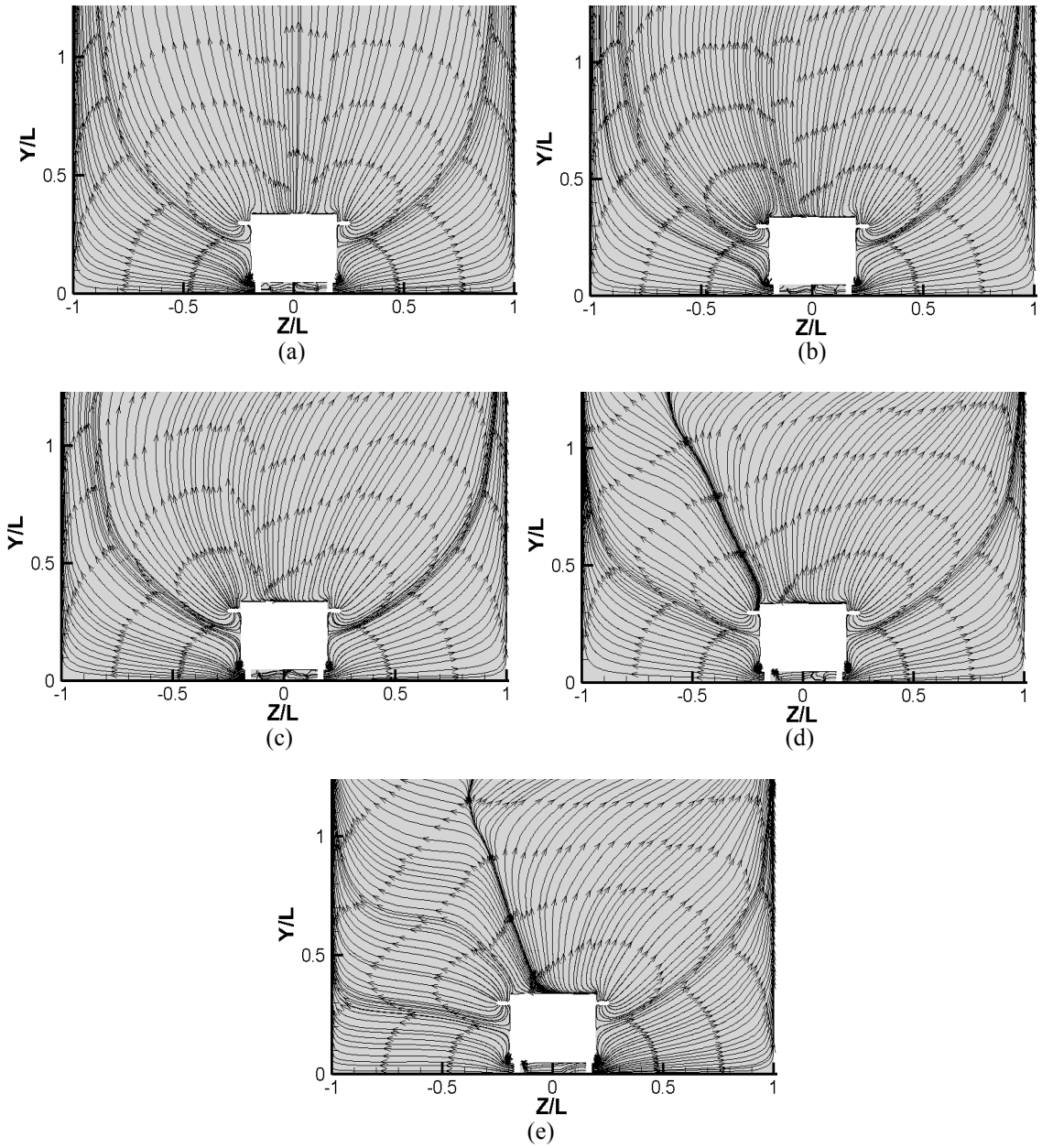

Figure 10. Streamlines velocity plane x=-0.8 for body with side devices at 40 m/s and 35° Slant angle (a: yaw angle 0°, b: yaw angle 5°, c: yaw angle 10°, d: yaw angle 20°, e: yaw angle 30°)

The vorticity magnitude is presented to show rear region of model for body without side device in Figure 11. When examining the figures, the vorticity magnitude is high at top and bottom of rear region of body. The magnitude also increases top region of model with increasing yaw angle. However, it can be observed that vorticity magnitude values reduce after flow has moved slightly away from rear region of model by increasing yaw angle.

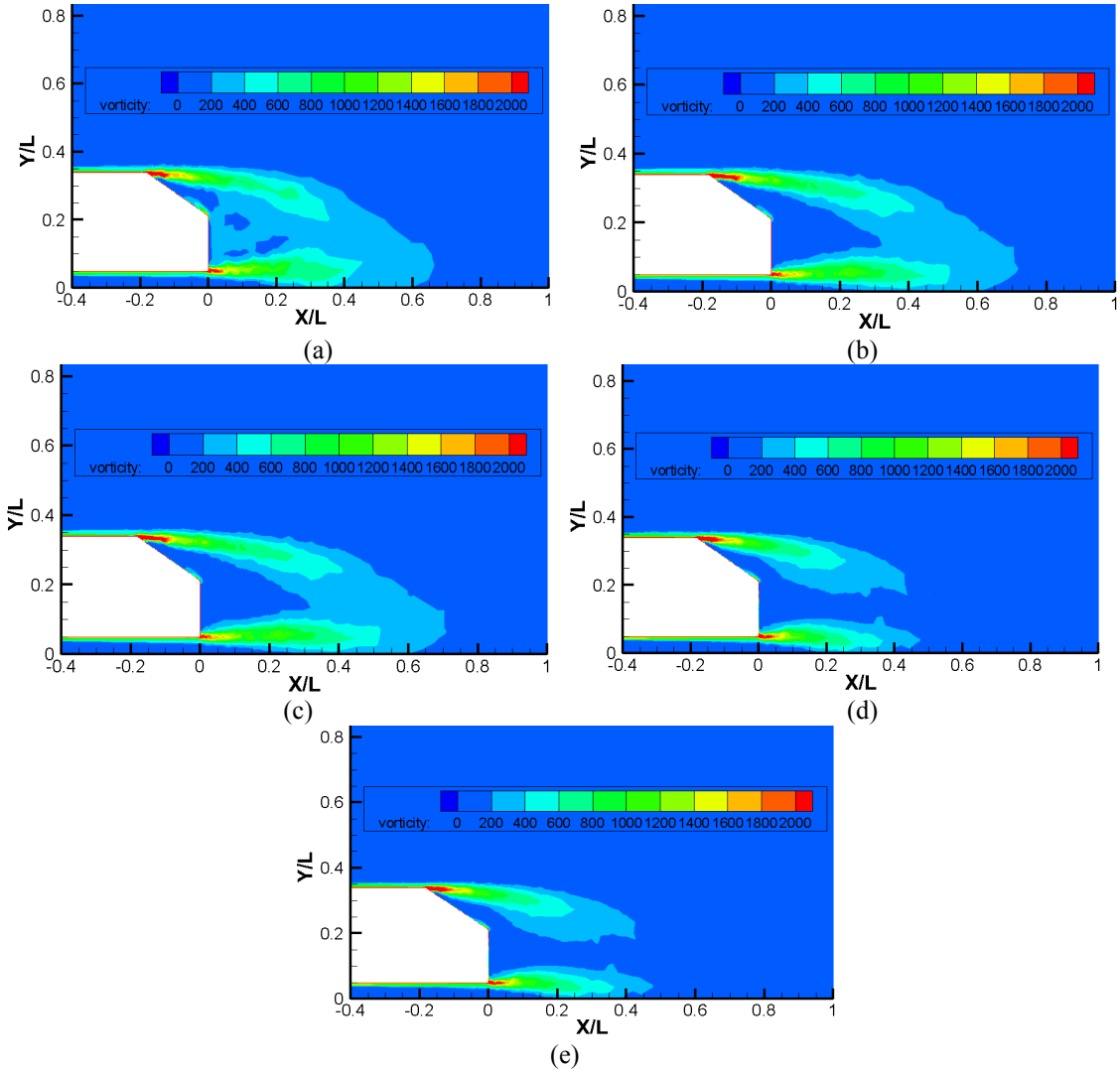

Figure 11. Vorticity magnitude for body without side devices at 40 m/s and 35° Slant angle (a: yaw angle 0°, b: yaw angle 5°, c: yaw angle 10°, d: yaw angle 20°, e: yaw angle 30°)

The CFD solution for without side devices of model was compared with previous study that reported C_D values [5] and it was concluded that the results were good agreement each other. Table 1 and Table 2 show the drag coefficients values for both models without and with side devices at 0°, 5°, 10°, 20° and 30° yaw angles, respectively.

Table 1. Drag values at 40 m/s and 35° slant angle without side device (a: yaw angle 0°, b: yaw angle 5°, c: yaw angle 10°, d: yaw angle 20°, e: yaw angle 30°)

Yaw Angles	**C_D Values**
0°	0,281
exp. results	**0,279 [5]**
5°	0,297
10°	0,321
20°	0,359
30°	0,388

Table 2. Drag values at 40 m/s and 35° slant angle with side device (a: yaw angle 0°, b: yaw angle 5°, c: yaw angle 10°, d: yaw angle 20°, e: yaw angle 30°)

Yaw Angles	C_D Values
0°	0,301
5°	0,312
10°	0,339
20°	0,368
30°	0,402

4. CONCLUSION

In the current study, side devices and crosswind effects were investigated for a simplified ground vehicle, separately since there are few studies related with both side device and crosswind analysis at the same time and different yaw angles when previous studies were examined. The model was generated using Designmodeler in ANSYS and the side devices were mounted on the model. The position and dimensions of side devices were determined by examining the previous studies [20, 21]. CFD solutions were then performed both cases in four different yaw angles (5°,10°,20° and 30°) because yaw angles of crosswind were generally studied at low, medium and high angles that are between 5° and 30° when previous papers were observed. In order to simulate flow field and capture boundary layer over Ahmed body, mesh generation was performed both prismatic and tetrahedral mesh structure and RNG k-ε turbulence model was used in Fluent solution.

Pressure contours were presented to show flow field at rear region of model and pressure drop or adverse pressure gradient were observed at slant surface of model due to effect of crosswind flow. The solution results were also presented as velocity streamlines at x-plane that is placed position of side devices. When the velocity streamlines were observed, the intensity and area of vortex formation are less than the model without side devices. Hence, crosswind flow causes the most of increase of aerodynamic drag force when compared with side device effect. However, the solution results with both crosswind and side device were showed that the drag force was more than the solution results with only crosswind effect. In addition, vorticity magnitude has been given for both without side devices at different yaw angle to observe vortex effects at rear region of model. Drag coefficients values were also presented for all solutions. The C_D values was compared with previous study that reported [5] and it was concluded that the results were good agreement each other. Finally, the results of solutions showed that side devices and crosswind reversely affected the body in point of aerodynamic performance since they cause air flow disruption and separation at rear region and side of model. The optimization study can be performed to find optimum position and dimensions of side device and increase aerodynamic performance for the future work.

5. REFERENCES

1. Ahmed, S. R., Ramm, G., Faltin, G., 1984. Some Salient Features of the Time-Averaged Ground Vehicle Wake. SAE Transactions, 473-503.
2. Ahmed, Syed R., 1981. Wake Structure of Typical Automobile Shapes. Transaction of the ASME, 162-169.
3. Lienhart, H., Becker, S., 2003. Flow and Turbulence Structure in the Wake of a Simplified Car Model. SAE Transactions, 785-796.
4. Watkins, S., Vino, G., 2008. The Effect of Vehicle Spacing on the Aerodynamics of a Representative Car Shape. Journal of Wind Engineering and Industrial Aerodynamics, 96(6-7), 1232-1239.
5. Meile, W., Brenn, G., Reppenhagen, A., Lechner, B., Fuchs, A., 2011. Experiments and Numerical Simulations on the Aerodynamics of the Ahmed Body. CFD Letters, 3(1), 32-39.
6. Östh, J., Noack, B.R., Krajnović, S., Barros, D., Borée, J., 2014. On the Need for a Nonlinear Subscale Turbulence Term in POD Models as Exemplified for a High-Reynolds-Number Flow over an Ahmed Body. Journal of Fluid Mechanics, 747, 518-544.

7. Volpe, R., Devinant, P., Kourta, A., 2015. Experimental Characterization of the Unsteady Natural Wake of the Full-scale Square Back Ahmed Body: Flow Bi-stability and Spectral Analysis. Experiments in Fluids, 56(5), 99.

8. Tunay, T., Firat, E., Sahin, B., 2018. Experimental Investigation of the Flow Around a Simplified Ground Vehicle under Effects of the Steady Crosswind. International Journal of Heat and Fluid Flow, 71, 137-152.

9. Tunay, T., Drugge, L., O'Reilly, C. J., 2020. On Coupling Methods Used to Simulate the Dynamic Characteristics of Heavy Ground Vehicles Subjected to Crosswind. Journal of Wind Engineering and Industrial Aerodynamics, 201, 104194.

10. McArthur, D., Burton, D., Thompson, M., Sheridan, J., 2018. An Experimental Characterisation of the Wake of a Detailed Heavy Vehicle in Cross-wind. Journal of Wind Engineering and Industrial Aerodynamics, 175, 364-375.

11. Lorite-Díez, M., Jiménez-González, J.I., Pastur, L., Cadot, O., Martínez-Bazán, C., 2020. Drag Reduction on a Three-Dimensional Blunt Body with Different Rear Cavities under Cross-Wind Conditions. Journal of Wind Engineering and Industrial Aerodynamics, 200, 104145.

12. Suzuki, M., Tanemoto, K., Maeda, T., 2003. Aerodynamic Characteristics of Train/vehicles under Cross Winds. Journal of Wind Engineering and Industrial Aerodynamics, 91(1-2), 209-218.

13. Guilmineau, E., Chometon, F., 2009. Effect of Side Wind on a Simplified Car Model: Experimental and Numerical Analysis. Journal of Fluids Engineering, 131(2).

14. Guilmineau, E., Chikhaoui, O., Deng, G., Visonneau, M., 2013. Cross Wind Effects on a Simplified Car Model by a DES Approach. Computers & Fluids, 78, 29-40.

15. Altınışık, A., Umur, H., 2018. Yanal Rüzgar Durumunda Otomobil Aerodinamiği. 9th International Automotive Technologies Congress OTEKON, 7-8 May, 2018, Bursa

16. Zafer, B., Haskaraman, F., 2017. Önden ve Yanal Rüzgar Şartı Altında Ahmed Cisminin Sayısal İncelenmesi. Journal of the Faculty of Engineering & Architecture of Gazi University, 32(1).

17. Bello-Millan, F.J., Mäkelä, T., Parras, L., Del Pino, C., Ferrera, C., 2016. Experimental Study on Ahmed's Body Drag Coefficient for Different Yaw Angles. Journal of Wind Engineering and Industrial Aerodynamics, 157, 140-144.

18. Tunay, T., Sahin, B., Ozbolat, V., 2014. Effects of Rear Slant Angles on the Flow Characteristics of Ahmed Body. Experimental Thermal and Fluid Science, 57, 165-176.

19. Kara, E., 2018. Numerical Investigation of Slant Angle Effect on a Simplified Car Model with Solution Adaptive Cartesian Grid Method. In International Congress of Automotive and Transport Engineering Springer, Cham. 32-39.

20. Muritala, A.O., Fatokun, H.A., Obayopo, S. O., 2017. Effect of an Add-on Device on the Aerodynamic Characteristics of a 3-Dimensional Ahmed Boyd. IOSR Journal of Mechanical and Civil Engineering, 14(6), 18-29.

21. Ensarioğlu, M.V., 2020. Taşitlarda Yan Ayna Üzerindeki Aerodinamik Etkilerin Nümerik Olarak İncelenmesi. Yüksek Lisans Tezi, Bursa Uludag Üniversitesi, Fen Bilimleri Enstitüsü, Makine Mühendisliği Anabilim Dalı, Bursa, 290.

22. Ahmed, A., Murtaza, M.A., 2016. CFD Analysis of Car Body Aerodynamics Including Effect of Passive Flow Devices–A REVIEW. International Journal of Research in Engineering and Technology, 5(3), 141-144.

23. Park, H., Cho, J.H., Lee, J., Lee, D.H., Kim, K.H., 2013. Aerodynamic Drag Reduction of Ahmed Model using Synthetic Jet Array. SAE International Journal of Passenger Cars-Mechanical Systems, 6(2013-01-0095), 1-6.

24. Buscariolo, F.F., Assi, G.R., Sherwin, S.J., 2021. Computational Study on an Ahmed Body Equipped with Simplified Underbody Diffuser. Journal of Wind Engineering and Industrial Aerodynamics, 209, 104411.

25. Yakkundi, V.K., Mantha, S.S., 2010. CFD Analysis of Flow over Car Variants & Validation with Ahmed Body. CURIE Journal, 3(1).

26. Demircioğlu, T.K., 2007. Bir Araç Modelinin Aerodinamik Analizi ve Sonlu Elemanlar Yöntemi ile Simülasyonu. Yüksek Lisans Tezi, Balıkesir Üniversitesi, Fen Bilimleri Enstitüsü, Makine Mühendisliği Anabilim Dalı, Balıkesir, 61.

27. Günay, C., Kumlutaş, D., Özer, Ö., Yücekaya, U.A., 2019. Elektrikli Arabalarin Aerodinamik Karakteristiklerinin Parçacik Görüntülemeli Hiz Ölçüm Yöntemi (Pghö) ve Sayisal Olarak İncelenmesi. 14. Ulusal Tesisat Mühendisliği Kongres, 17-20 Nisan, 2019, İzmir.

28. Han, T., 1989. Computational Analysis of Three-dimensional Turbulent Flow Around a Bluff Body in Ground Proximity. AIAA Journal, 27(9), 1213-1219.

29. Krastev, V.K., Bella, G., 2011. On the Steady and Unsteady Turbulence Modeling in Ground Vehicle Aerodynamic Design and Optimization. SAE Technical Paper, No. 2011-24-0163.

30. Hinterberger, C., Garcia-Villalba, M., Rodi, W., 2004. Large Eddy Simulation of Flow Around the Ahmed Body. In The Aerodynamics of Heavy Vehicles: Trucks, Buses, and Trains, Springer, Berlin, Heidelberg, 77-87.

31. Jermann, C., Pujals, G., Meliga, P., Serre, E., Gallaire, F., 2013. Characterization of the Streamwise Vortices and Near-wake Dynamics in the Turbulent Flow Around the 25° Ahmed Body Based on SPIV. In 3rd GDR Symposium "Flow Separation Control", Ecole Centrale de Lille, 7th and 8th, 2013.

32. Dumas, L., 2008. CFD-Based Optimization for Automotive Aerodynamics. In Optimization and Computational Fluid Dynamics. Springer, Berlin, Heidelberg, 191-215.

33. Beigmoradi, S., Hajabdollahi, H., Ramezani, A., 2014. Multi-Objective Aero Acoustic Optimization of Rear end in a Simplified Car Model by using Hybrid Robust Parameter Design, Artificial Neural Networks and Genetic Algorithm Methods. Computers & Fluids, 90, 123-132.

34. He, P., Mader, C.A., Martins, J.R., Maki, K.J., 2018. An Aerodynamic Design Optimization Framework using a Discrete Adjoint Approach with OpenFOAM. Computers & Fluids, 168, 285-303.

35. Han, T., Hammond Jr, D.C., Sagi, C.J., 1992. Optimization of Bluff Body for Minimum Drag in Ground Proximity. AIAA Journal, 30(4), 882-889.

36. Wang, Y., Wu, C., Tan, G., Deng, Y., 2017. Reduction in the Aerodynamic Drag Around A Generic Vehicle by using a Non-Smooth Surface. Proceedings of the Institution of Mechanical Engineers. Part D: Journal of Automobile Engineering, 231(1), 130-144.

37. Qiao, Z.X., Minelli, G., Noack, B.R., Krajnović, S., Chernoray, V., 2021. Multi-Frequency Aerodynamic Control of a Yawed Bluff Body Optimized with a Genetic Algorithm. Journal of Wind Engineering and Industrial Aerodynamics, 212, 104600.

38. Kalaycı, C., 2021. SUV Model Bir Motorlu Taşıtın Aerodinamik Performansının Sayısal İncelenmesi ve Optimizasyonu. Yüksek Lisans Tezi, Batman Üniversitesi, Lisansüstü Eğitim Enstitüsü, Makine Mühendisliği Anabilim Dalı, Batman, 63.

39. Şumnu, A., 2021. Shape Modification of Ahmed Body to Reduce Drag Coefficient and Determination of Turbulence Model. Niğde Ömer Halisdemir Üniversitesi Mühendislik Bilimleri Dergisi, 10(2), 824-832.